

Mechanical Behavior and Constitutive Modeling of Cement–Bentonite Mixtures for Cutoff Walls

*Original*

Mechanical Behavior and Constitutive Modeling of Cement–Bentonite Mixtures for Cutoff Walls / Flessati, Luca; Della Vecchia, Gabriele; Musso, Guido. - In: JOURNAL OF MATERIALS IN CIVIL ENGINEERING. - ISSN 0899-1561. - STAMPA. - 33:3(2021), pp. 1-12. [[10.1061/\(ASCE\)MT.1943-5533.0003584](https://doi.org/10.1061/(ASCE)MT.1943-5533.0003584)]

*Availability:*

This version is available at: [11583/2857538](https://doi.org/10.1061/(ASCE)MT.1943-5533.0003584) since: 2021-01-09T19:26:25Z

*Publisher:*

ASCE

*Published*

DOI:[10.1061/\(ASCE\)MT.1943-5533.0003584](https://doi.org/10.1061/(ASCE)MT.1943-5533.0003584)

*Terms of use:*

This article is made available under terms and conditions as specified in the corresponding bibliographic description in the repository

*Publisher copyright*

(Article begins on next page)

1                   **Mechanical behavior and constitutive modeling of**  
2                   **cement-bentonite mixtures for cutoff walls**

3                   Luca Flessati<sup>1</sup>, Gabriele Della Vecchia<sup>2</sup>, and Guido Musso<sup>3</sup>

4                   <sup>1</sup>Department of Civil and Environmental Engineering, Politecnico di Milano, Piazza  
5                   Leonardo da Vinci 32 Milano, Italy

6                   <sup>2</sup>Department of Civil and Environmental Engineering, Politecnico di Milano, Piazza  
7                   Leonardo da Vinci 32 Milano, Italy Email: luca.flessati@polimi.it

8                   <sup>3</sup>Department of Structural, Geotechnical and Building Engineering, Politecnico di Torino,  
9                   Corso Duca degli Abruzzi 24 Torino, Italy

10                  **ABSTRACT**

11                  Cement-bentonite mixtures are commonly used to build cutoff walls which limit water  
12                  flow and underground transport of pollutants. These artificial materials are employed due  
13                  to their very low permeability and adequate shear strength and ductility. In this paper, ex-  
14                  perimental results about the microstructure and the mechanical behavior of three different  
15                  cement-bentonite mixtures are presented. Specimens of these mixtures were subjected to  
16                  oedometer and consolidated-undrained triaxial tests. These results were then used as a basis  
17                  for the definition of a suitable constitutive framework. A quite good reproduction of the  
18                  experimental results up to the peak strength was obtained using the classical Modified Cam  
19                  Clay model, which could then be used satisfactorily when conventional analyses aimed at  
20                  assessing the stability of cutoff walls are required. The reproduction of the strength degra-  
21                  dation and the strains occurring in the post peak stage requires however a more advanced  
22                  constitutive model. To this extent, Modified Cam Clay framework was enhanced by intro-  
23                  ducing some features commonly employed to reproduce the mechanical behavior of granular

24 materials. This model may be useful for the real scale analysis of more critical cases, when  
25 local failure mechanisms are likely to occur and may influence the functionality of the wall.

## 26 INTRODUCTION

27 In environmental geotechnics, barriers are often designed for seepage control and for  
28 the isolation of pollutants that may contaminate the groundwater. Cutoff walls are one of  
29 the most widespread solutions (Opdyke and Evans 2005; Joshi et al. 2010; Jefferis 2012;  
30 Royal et al. 2013; Soga et al. 2013; Carreto et al. 2016). **They are often built with**  
31 **cement-bentonite mixtures.** These artificial materials are used because of their very low  
32 permeability, but also because the construction processes they require are very simple. The  
33 cement-bentonite **mixture** in a slurry state fills a trench while this is excavated around the  
34 contaminated zone, remaining fluid along the whole excavation phase. Later on, the same  
35 mixture sets and hardens while left in the trench, forming a material with the required hydro-  
36 mechanical properties. According to Carreto et al. (2016), pure cement-bentonite mixtures  
37 are suitable for applications in which the required permeability is of the order of  $10^{-8}$  m/s,  
38 i.e. for water seepage control. To further reduce the permeability and to increase durability  
39 with respect to chemicals in the groundwater, in many cases part of the cement is replaced  
40 with slag (Opdyke and Evans 2005; Royal et al. 2013; Soga et al. 2013; Royal et al. 2018).

41 Cement-bentonite mixtures are employed because of their low permeability, but a cut-  
42 off wall is also required to possess a shear strength roughly equivalent to the surrounding  
43 soils, and, more importantly, it should be sufficiently ductile so that cracks do not develop  
44 if the wall is subject to large strains under confined stress conditions. Thus, attention  
45 on the stress-strain behavior of containment walls is needed in order to avoid loss of cutoff  
46 performance. Typically, wall specifications call for a sample of the cement-bentonite mixture  
47 to accommodate a strain of at least 5% without cracking failure, despite in practice the  
48 ability of cement-bentonite to withstand these strains under drained conditions is rarely  
49 a problem, with values often in excess of 10% being achieved (Jefferis 1981). However,  
50 the brittle behavior shown by cement-bentonite mixtures at low confining stresses during

51 undrained triaxial loading (Soga et al. 2013; Carreto et al. 2016; Royal et al. 2018) may be  
52 critical for the barrier performance, as softening is related to the development of localized  
53 failures that could lead to preferential paths for water flow. While the hydraulic behavior of  
54 these mixtures has been investigated in detail, studies on the mechanical behavior have been  
55 mostly limited to the assessment of the material strength and constitutive models capable  
56 of assessing both material strength and strains at failure are lacking.

57 In this paper, **the results of an experimental study on the mechanical behavior**  
58 **of three different cement-bentonite mixtures are presented**, including oedometer and  
59 consolidated-undrained triaxial tests. The experimental results were exploited to evaluate the  
60 possible use of suitable constitutive mechanical models. The use of the Modified Cam Clay  
61 (MCC) model (Roscoe and Burland 1968) is first discussed. The MCC was chosen especially  
62 in light of its practicality, since (i) it requires a small number of constitutive parameters with  
63 clear physical meaning, (ii) the procedures to calibrate the constitutive parameters are well  
64 established and (iii) it is implemented in most numerical geotechnical codes. An enhanced  
65 model, introduced to improve the reproduction of aspects that are not very well handled by  
66 the MCC such as strength degradation, excess pore pressure evolution upon shearing and  
67 strain at failure, is then described. Such an advanced model is an original proposal and it  
68 was obtained by introducing in the MCC framework some features commonly employed to  
69 reproduce the undrained mechanical response of granular materials (Li and Dafalias 2000).  
70 This new model may be adopted in critical cases, when local failure mechanisms are likely to  
71 occur and may influence the functionality of the wall. The performance of both constitutive  
72 models was checked against both the experimental results reported in this work and against  
73 the ones in Carreto et al. (2016).

## 74 **EXPERIMENTAL TESTS**

75 In this section, the results of the experimental tests performed in the Geotechnical Lab-  
76 oratory of Politecnico di Torino are presented and discussed. After describing the procedure  
77 followed to obtain the cement-bentonite specimens, some photomicrographs of microstruc-

78 ture are presented together with experimental results of oedometer and triaxial tests.

## 79 **Specimen preparation**

80 The cement-bentonite slurries were prepared by mixing water, a sodium bentonite from  
81 Laviosa Mineraria (specific gravity 2.95, liquid limit 535%, plastic limit 75%) and Portland  
82 cement (CEM I 32.5N). Three different slurry compositions were considered (hereafter named  
83 CB4, CB5 and CB6) prepared by mixing in different proportions cement ( $C$ ), bentonite ( $B$ )  
84 and water ( $W$ ). The mass ratios used in the preparations are summarized in Table 1.

85 Preparation occurred in three steps: (i) water and bentonite were mixed by means of  
86 a laboratory mixer, (ii) after 24h, required for the bentonite hydration, cement was added  
87 and the slurry was mixed again and (iii) the mixtures were poured into cylindrical molds  
88 (Figure 1), having the size required to prepare the specimens for mechanical testing. The  
89 specimens were immersed in water, where they were cured for 28 days. During this last  
90 phase the specimens hardened and also consolidated under their self weight. Further details  
91 on the preparation of the specimens can be found in (Tarzia 2018).

92 After curing, the water content ( $w$ ) and the specific gravity ( $G_s$ ) were measured by means  
93 of standard laboratory tests (ASTM (2019) Designation:D2216–19 and ASTM (2014)  
94 Designation:D854–14, respectively). These values (Table 1) were employed to calculate  
95 the initial void ratio  $e_0$  (Table 1) of the specimens of the different mixtures. Because of the  
96 presence of the cement and the reactions between water, bentonite and cement, the void  
97 ratio of the mixture is significantly lower than the one of the bentonite slurry (this one being  
98 equal to 22). As shown in Table 1, the higher the cement bentonite ratio, the lower the  
99 initial void ratio.

## 100 **Investigation at the micro scale**

101 The microstructure of specimens of the different mixtures was investigated by means of  
102 Scanning Electron Microscope (SEM) pictures, at magnifications ranging from 400 to 20000  
103 fold the original. During SEM analyses, a vacuum condition must be imposed within the  
104 chamber and only dry, or nearly dry, specimens can be introduced. However, it has been

105 shown that the evaporation of water from Cement Bentonite occurring at room conditions has  
106 a significant impact on the material behavior, since it causes irreversible shrinkage (Trischitta  
107 et al. 2020) and the generation of cracks (Musso et al. 2020b). Limited experimental evidence  
108 also shows that such water evaporation reduces strength (Royal et al. 2018). All these  
109 evidences suggest that the fabric alters significantly when the mixture undergoes evaporation.  
110 To this extent, the SEM specimens were prepared following the same procedure used for the  
111 microstructural investigation of soil specimens (Delage and Pellerin 1984; Azizi et al. 2020).  
112 Dehydration was thus imposed through freeze-drying cycles, which, contrarily to evaporation,  
113 cause very limited changes to the original fabric.

114 **The difference in terms of SEM images encountered between specimens of**  
115 **different mixtures was very small. For this reason, CB5 is selected as represen-**  
116 **tative and SEM images of CB5 after curing are shown in Figure 2.** At a 400 fold  
117 magnification (photograph in the left upper corner, bar length 300 microns) the microstruc-  
118 ture appears to consist of roughly spherical elements, which are quite densely connected one  
119 with the other through a rather homogeneous fabric. These spherical elements have diameter  
120 of the order of a few tens of microns (silt size). A number of **pores** having a diameter of  
121 the order of about ten microns are present, as it can be appreciated at a 800 fold magnifi-  
122 cation (photograph in the right upper corner, bar length 100 microns). It is not possible to  
123 distinguish between the original clay platelets and the cementitious material.

124 **Energy Dispersive X-ray microanalysis, run during SEM imaging on different**  
125 **parts of the specimen, detected atoms of Calcium, Silicon, Oxygen, Aluminum,**  
126 **Carbon and Magnesium (Figure 3). It was not possible to find a significant**  
127 **difference between the composition of solids on basis of their shape or size;**  
128 **furthermore the species that were found are bricks of the mineralogy of both**  
129 **cement and bentonite.** No Sodium was detected, although this is a primary constituent  
130 of the original mineralogy of the bentonite. **On the contrary, Sodium was found to**  
131 **be abundant in the pore water, suggesting that cation exchange (Calcium for**

132 **Sodium**) might have occurred within the clay, consistently with the observations  
133 presented in (Kang et al. 2015). Due to the cement hydration reactions, the pore water  
134 within the specimens had a pH=12. Altogether, the high pH of the pore water and the  
135 prevalence of an exchangeable divalent cation (Calcium) in the bentonite structure, promote  
136 the aggregation of the bentonite particles into aggregates (van Olphen 1977). The “particles”  
137 observed at the 400 and 800 fold magnifications are then likely to be bentonite aggregates,  
138 more or less effectively “coated” by the cement. This justifies the large pores, which otherwise  
139 would be rather unusual for active clays such as bentonite.

140 The larger “silty elements” are found to be assemblages of hardened cement particles  
141 and aggregates of clay particles coated by cement, as it is appreciated at the 5000 fold  
142 magnification (left bottom picture). A field of **randomly** disposed ettringite needles, which  
143 do not form a clear reticular structure, grow between the particles and aggregates (right  
144 bottom picture).

145 On the overall, the observed fabric is very different from the one typical of bentonites,  
146 and despite the low permeability of the material, it is more similar to the one of a multiscale,  
147 silty-like, cemented material. Although the experimental observations here collected refer  
148 to specimens that were cured for 28 days, they are very consistent with the findings in Plee  
149 et al. (1990), which restricted the investigation to the first 24 hours of ageing.

## 150 **Oedometer test results**

151 The results of the oedometer tests performed on the three different mixtures, described  
152 in Tarzia (2018), are plotted in Figure 4 in the  $e - \sigma'_v$  compression plane (being  $e$  and  $\sigma'_v$  the  
153 void ratio and the applied vertical effective stress, respectively). The experimental results  
154 allow identifying a vertical stress value corresponding to a sudden change in compressibility.  
155 This vertical stress, named in the geotechnical literature “preconsolidation pressure”, is  
156 interpreted as a yield stress according to the generally adopted framework of elasto-plasticity.  
157 It is worth noting that the mixture tested is virgin from the mechanical point of view,  
158 implying that the yielding point is associated with the bonding provided by the cement

rather than to over-consolidation. According to Figure 4, the value of the preconsolidation stress increases with the cement content, being of the order of 30 kPa for the CB4 specimen and about 80 kPa and 140 kPa respectively for the CB5 and CB6 ones. **The experimental results also highlight that the slopes of the virgin loading branch is slightly affected by the cement content, with  $C_c$  values ranging from 3.5 for mixture CB4 to 3 for mixture CB6. The compression index  $C_c$  is defined as the slope of the virgin branch of the compression curve in the  $e - \log \sigma'_v$  plane. The ratio between the compression index  $C_c$  and the swelling index ( $C_s = 0.08$ , defined as the slope of the unloading branch of the compression curve in the  $e - \log \sigma'_v$  plane) is very large and on the average it is approximately equal to 40.** The role of cement appears more relevant if the compressibility is compared to the one of the pure bentonite. In that case, the measured values of  $C_c$  and  $C_s$  were equal to 7.9 and 3.9, respectively. This clearly puts in evidence that the presence of the cement significantly increases the stiffness and makes more evident the difference between mixture response during virgin loading and unloading. Interestingly, the slope of the initial branch of the compression curve (i.e. for vertical stress values lower than the preconsolidation one) is quite similar to the slope of the unloading branch. This may suggest that during these stages the variation of void ratio can be related to the same microstructural process, like the compressibility of cement-bentonite clusters. Moreover, the evidence that the elastic compressibility does not change after virgin loading, i.e when a spatial rearrangement of clusters certainly takes place, suggests that the bonds provided by the cement have not been significantly damaged during virgin loading.

### Consolidated undrained triaxial tests

Consolidated undrained triaxial (TXCU) tests were run on the three different cement-bentonite mixtures (Tarzia 2018). The specimens were first isotropically consolidated at different confining pressure values. A backpressure was applied to ensure the full saturation of the specimens. **The confining pressure ( $p_c$ ) is the difference between the cell pressure and the back pressure.** The experimental results obtained for  $p_c=20, 100$  and



186 300 kPa are shown in Figures 5a-c. In particular, the results are plotted in (i) the  $q - \varepsilon_a$  plane  
187 (being  $\varepsilon_a$  the imposed axial strain,  $q = \sigma'_v - \sigma'_h$  the deviator stress whereas  $\sigma'_h$  is the horizontal  
188 effective stress, respectively), (ii) the  $\Delta u - \varepsilon_a$  plane (being  $\Delta u$  the excess pore water pressure  
189 accumulated during shearing) and (iii) in the  $q - p'$  plane (being  $p' = (\sigma'_v + 2\sigma'_h)/3$  the average  
190 effective stress).

191 The experimental results reported in Figure 5a ( $p_c = 20$  kPa) put in evidence a similar  
192 response of specimens constituted of mixtures CB5 and CB6: the deviator stress increases  
193 monotonically up to an asymptotic value, whereas the initial increase of excess pore water  
194 pressure is followed by a decreasing branch, starting from an axial strain approximately equal  
195 to 1%. For both mixtures, the preconsolidation stress, identified along the compression curve  
196 (Figure 4), is significantly larger than the confining pressure applied during the consolidation  
197 stage of the triaxial test  $p_c$ : undrained shear is in this case applied to “highly overconsol-  
198 idated” specimens. On the contrary, the preconsolidation stress for the CB4 specimen (as  
199 shown in Figure 4) is not significantly larger than the imposed  $p_c$  value: the specimen is in  
200 this case is “lightly overconsolidated” and both  $q$  and  $\Delta u$  are monotonically increasing with  
201  $\varepsilon_a$  up to an asymptotic value.

202 The experimental results reported in Figures 5b and 5c are obtained for  $p_c$  values which  
203 are at least similar (Fig 4, CB6) or larger than the preconsolidation stress. In this case, the  
204 three specimens are normally consolidated and the type of undrained mechanical response  
205 seems not significantly affected by the C/B ratio. In the  $q - \varepsilon_a$  plane a peak, followed by  
206 a decrease of the deviatoric stress, is evident. After the peak, excess pore water pressure  
207 remains constant. This implies that, analogously to what was obtained by Carreto et al.  
208 (2016), the decreasing branch of the effective stress path in the  $q - p'$  plane is characterized  
209 by a slope equal to 3:1 (i.e. the same of the total stress path during the shear stage of triaxial  
210 tests).

211  
212 **A conventional interpretation of the strength of the different mixtures was**

213 made in terms of Mohr-Coulomb envelopes, plotted in Figure 6. Towards the  
 214 end of the tests, all the specimens of the different mixtures tended to a critical  
 215 state condition. The ultimate (final) strength envelope was interpreted with the  
 216 equation:

$$217 \quad q = Mp' \quad (1)$$

218 For the CB4 mixture, it was found that the strength ratio  $q/p'$  increased  
 219 monotonically with axial strain for all of the specimens, and there was no need  
 220 to define a peak strength. On the contrary, for the CB5 and CB6 mixtures, the  
 221  $q/p'$  ratio showed a peak value at smaller strains before tending to the critical  
 222 state at the end of the tests. This was particularly evident for the “highly  
 223 overconsolidated” specimens tested at a confining pressure of 20 kPa. For these  
 224 mixtures, a peak envelope was also defined, expressed as:

$$225 \quad q = I + \eta_{max}p' \quad (2)$$

226 The parameters of Equations 1 and 2 can be related to the constant volume  
 227 friction angle  $\phi'_{cv}$ , the peak strength angle  $\phi'_p$  and to the cohesion intercept  $c'_p$   
 228 (which might be of more common use in the engineering practice than  $M$ ,  $\eta_{max}$   
 229 and  $I$ ), through equations:

$$230 \quad M = \frac{6 \sin \phi'_{cv}}{3 - \sin \phi'_{cv}} \quad \eta_{max} = \frac{6 \sin \phi'_p}{3 - \sin \phi'_p} \quad c'_p = I \cdot \frac{3 - \sin \phi'_p}{6 \cos \phi'_p} \quad (3)$$

231 The peak  $q/p'$  ratio of mixtures CB5 and CB6 decreases with the confin-  
 232 ing pressure, as expected to occur in soils as the degree of overconsolidation is  
 233 reduced (see e.g. [Atkinson and Bransby \(1978\)](#)). The values of the strength  
 234 parameters for the peak and the ultimate conditions are provided in Table 2.  
 235 Interestingly, the friction angles slightly decrease as the cement/bentonite ratio

236 increases, while the cohesion increases with the cement/bentonite ratio.

## 237 CONSTITUTIVE MODELING

238 When dealing with cutoff wall behavior, chemo-hydraulic simulations are generally per-  
239 formed, neglecting the role of the mechanical response on the transport properties of the mix-  
240 ture. However, if deformation and stability issues are of concern, a mathematical formulation  
241 of the stress-strain response is needed. **In this section, the use of two different con-**  
242 **stitutive relationships to simulate the mechanical response of cement-bentonite**  
243 **mixtures, both of them in the framework of strain-hardening elasto-plasticity,**  
244 **is explored.** These are the standard Modified Cam Clay model (MCC) and an enhanced  
245 version of the MCC (CBC in the following), which was developed to improve predictions  
246 especially in the post peak branch.

### 247 Modified Cam Clay model

248 The Modified Cam Clay model is one of the most widespread constitutive models used  
249 in geotechnical engineering. It has been developed to simulate the mechanical behavior of  
250 saturated reconstituted clays, but its range of applicability has been extended to many other  
251 materials by properly adjusting the original formulation. The MCC model is an elastic-  
252 plastic model, characterized by isotropic hardening. When the stress state lies inside the  
253 yield locus or during unloading, material response is elastic: MCC assumes an isotropic non-  
254 linear elastic response, with a pressure dependent elastic bulk modulus ( $K$ ) and a constant  
255 Poisson ratio ( $\nu$ ). The bulk modulus  $K$  is expressed as:

$$256 \quad K = \frac{1 + e_0}{\kappa} p', \quad (4)$$

257 being  $\kappa$  is the slope of the unloading-reloading line in the  $e - \ln p'$  plane.

258 In elasto-plasticity, the direction of the plastic strain increments is ruled by the plastic  
259 potential function ( $g$ ). In associated plasticity, the yield function ( $f$ ) and the plastic potential  
260 ( $g$ ) are coincident. For the MCC, they are both ellipses in the  $q - p'$  plane, expressed as:

$$f = g = \frac{q^2}{M^2} - p'(p'_s - p'), \quad (5)$$

where  $M$  and  $p'_s$  are the slope of the critical state line in the  $q-p'$  plane and the hardening variable, respectively.

The increment of the hardening variable is defined according to the experimental evidence of material virgin compression along oedometer or isotropic paths:

$$\frac{\partial p'_s}{\partial \varepsilon_{vol}^{pl}} = \frac{1 + e_0}{\lambda - \kappa} p'_s \quad (6)$$

being  $\lambda$  the inclination of the Normal Compression Line in the  $e - \ln p'$  plane and  $\varepsilon_{vol}^{pl}$  the volumetric plastic strain.

By imposing the consistency conditions, the hardening modulus can be derived:

$$H = -\frac{\partial f}{\partial p'_s} \frac{\partial p'_s}{\partial \varepsilon_{vol}^{pl}} \frac{\partial g}{\partial p'} = (p') \left( \frac{1 + e_0}{\lambda - \kappa} p'_s \right) (2p' - p'_s) \quad (7)$$

The hardening modulus, defining whether the material hardens ( $H > 0$ ) or softens ( $H < 0$ ), puts in evidence that hardening takes place when  $p' > p'_s/2$  (“wet” clays according to Roscoe and Burland (1968)) whereas softening when  $p' < p'_s/2$  (“dry” clays according to Roscoe and Burland (1968)). In case  $p' = p'_s/2$ ,  $H = 0$  and the material is at critical state, i.e. the material accumulates deviatoric plastic strains without changing its volume and state of stress.

### *Parameter calibration and model predictions*

To calibrate the model, the values of four constitutive parameters ( $\nu$ ,  $\kappa$ ,  $\lambda$  and  $M$ ) and the initial value of the void ratio and the hardening variable ( $e_0$  and  $p'_{s0}$ ) have to be defined.

The initial void ratio values are taken from Table 1. The Poisson ratio value was assumed to be equal to 0.25, a realistic value for geotechnical analyses. The values of  $\kappa$ ,  $\lambda$  and  $p'_{s0}$  were calibrated on the basis of the compression curve in oedometer conditions:  $\kappa$  was calibrated on the slope of the unloading branch,  $\lambda$  on the slope of the virgin branch and  $p'_{s0}$  where

284 the transition between the reloading and the virgin loading response takes place (Figures  
285 7a-c). The MMC constitutive equations were integrated under oedometer stress paths (nil  
286 horizontal strains and an imposed vertical stress history) and the values of  $\kappa$ ,  $\lambda$  and  $p'_{s0}$   
287 were changed until a satisfactory agreement between the experimental results and the MMC  
288 prediction was obtained (Figure 7a-c).

289 **The calibrated values of the relevant parameters of the MMC model for the**  
290 **three mixtures are listed in Table 3 (CB4, CB5 and CB6). M values were taken**  
291 **from Table 2.**

292 The results of the undrained triaxial tests plotted in the  $q - \varepsilon_a$  and the effective stress  
293 paths in the  $q - p'$  plane were not directly exploited to calibrate the constitutive parameters,  
294 so that the experimental results in these planes may be employed for model validation. The  
295 comparison between experimental results (dotted lines) and the results obtained by numer-  
296 ically integrating the MMC model constitutive equations along an undrained triaxial stress  
297 path (solid lines) is reported in Figures 8-10. The MCC model satisfactorily reproduces the  
298 material mechanical response up to the peak deviator stress, but it is not able to reproduce  
299 the strength reduction. The dashed lines of Figures 8-10 will be commented in the following  
300 section.

301 A further verification on the validity of the MCC model to predict the behavior of these  
302 mixtures was done by simulating the tests reported in [Carreto et al. \(2016\)](#). In that paper  
303 the authors performed a series of isotropic compression and undrained triaxial tests on  
304 different cement-bentonite mixtures. For the sake of brevity, only one mixture composition  
305 (composition A in [Carreto et al. \(2016\)](#), W/B=28.6 and C/B=5.71) is hereafter discussed.

306 Analogously to the previous case,  $M$  was calibrated on final points of the effective stress  
307 paths and the Poisson ratio is assumed to be equal to 0.25, while  $e_0$ ,  $\kappa$ ,  $\lambda$  and  $p'_{s0}$  were  
308 calibrated on the isotropic compression test results. The values of the parameters are also  
309 summarized in Table 3.

310 The comparison between the experimental undrained triaxial test results corresponding

311 to  $p'_c=100, 200$  and  $400$  kPa (dotted lines) and the results obtained by integrating MCC con-  
312 stitutive equations (solid lines) is reported in Figure 11. Also in this case, the reproduction  
313 of the experimental results is very satisfactory up to the peak deviatoric stress. The dashed  
314 line of Figure 11 will be commented in the following section.

315 It is worth mentioning that the mixture employed by Carreto et al. (2016) is different  
316 with respect to the one studied in this paper (Table 1). Even if the composition in terms of  
317 C/B ratio value is similar to the one corresponding to mixture CB6, the initial void ratio and  
318 the initial value of the hardening variable are similar to the one obtained for mixture CB4.  
319 Moreover, the values of  $\lambda$  and  $\kappa$ , associated with the material compliance, are larger with  
320 respect to the ones obtained for the mixtures studied in this paper. **These differences are**  
321 **likely due to the significantly larger W/B ratio value of the mixture employed**  
322 **by Carreto et al. (2016).**

### 323 **Enhancement of MCC for cement-bentonite**

324 Both the stress strain and the stress path plots in Figures 6-9 show that the MMC  
325 model allows a good estimation of the material strength and an adequate reproduction of  
326 the pre-failure behavior. Nevertheless, the reproduction of the post-failure behavior is rather  
327 poor. This is especially true with the specimens tested at higher confining pressures, which  
328 showed a noticeable loss of strength as the axial strains progressed. Remarkably, this is  
329 often associated to localized failure, which would affect the integrity of the barrier causing  
330 preferential flow paths. It follows that the use of the MCC in the design of cutoff walls  
331 exposed to high mechanical solicitations might result unsafe, since it would not account for  
332 possible increase in the hydraulic conductivity of the barrier and loss of performance. A  
333 more advanced constitutive model should then be preferred.

334 **To be able to reproduce the post-peak behavior, a novel strain hardening**  
335 **elastic-plastic constitutive model, hereafter named Cement Bentonite Consti-**  
336 **tutive model (CBC model), is introduced. In particular, the capabilities of the**  
337 **MCC were enhanced by using mathematical laws, related both to plastic flow and**

338 hardening, inspired to existing relationships originally formulated for granular  
339 materials. This was motivated by the microstructural evidence discussed in the  
340 previous chapter and the experimental results of undrained triaxial tests. The  
341 clusters acting as solid grains convey the cement-bentonite mixture an undrained  
342 behavior that is very similar to the one of granular materials, namely: (i) progres-  
343 sive loss of strength when the material is in a ‘normal-consolidated’ loose state  
344 (i.e. when the void ratio is high with reference to the current confining pressure)  
345 and (ii) a ductile response when the material is in an ‘over-consolidated’ dense  
346 state (i.e. when the void ratio is low with reference to the current confining  
347 pressure). Notably, a similar approach was recently adopted by [Musso et al. \(2020a\)](#), to  
348 reproduce the mechanical behavior of unsaturated clayey silts.

349 For the sake of simplicity, the elastic law and the yield function are assumed to be the  
350 same of the MCC model, but the flow rule is assumed to be non-associated (i.e. the plastic  
351 potential and the yield function do not coincide). According to ([Manzari and Dafalias  
352 1997](#); [Li and Dafalias 2000](#); [Dafalias and Manzari 2004](#)), the flow rule is expressed in terms  
353 of dilatancy  $d$ , defined as the ratio between the incremental volumetric plastic strain and  
354 the incremental deviatoric plastic strain. In particular, following [Li and Dafalias \(2000\)](#),  
355 dilatancy is assumed to depend not only on the stress obliquity  $\eta = q/p'$  and  $M$  (like in  
356 the MCC model), but also on a scalar quantity  $\psi$  ([Been and Jefferies 1985](#)), named state  
357 parameter. In this paper,  $\psi$  is assumed to be a variable describing the distance (in term of  
358 void ratio) from the current material state (defined in terms of  $e$  and  $p'$ ) with respect to the  
359 corresponding critical state. It is defined as:

$$360 \quad \psi = e - \left( \Gamma - \lambda \ln \frac{p'}{p_{ref}} \right) \quad (8)$$

361 where  $p_{ref} = 1kPa$ , whereas  $\Gamma$  and  $\lambda$  describe the critical state locus in the  $e - p'$  plane.  
362 This latter is a straight line in the semilogarithmic  $e - p'$  plane:  $\lambda$  represents its slope,  
363 whereas  $\Gamma$  is the (critical) void ratio for  $p' = p_{ref}$ . Analogously to what proposed in [Li and](#)

364 [Dafalias \(2000\)](#) for dilatancy evolution in sands, the following expression is adopted:

$$365 \quad d = M \exp(g_1 \psi) - \eta, \quad (9)$$

366 where  $g_1$  is a (positive) non-dimensional constitutive parameter. As for the hardening  
367 rule, it was again assumed to depend on  $\eta$ ,  $M$  and  $\psi$ . The following plastic hardening  
368 modulus is thus proposed:

$$369 \quad H = \left( p'_s \frac{1 + e_0}{\lambda - \kappa} \right) h_1 \left[ \frac{M}{\eta} - \exp(h_2 \psi) \right] \quad (10)$$

370 where  $h_1$  and  $h_2$  are two (positive) non-dimensional constitutive parameters. In Equation  
371 10, the term  $(p'_s(1 + e_0)/(\lambda - \kappa))$  is the same appearing in the MMC hardening modulus  
372 (Equation 7), describing isotropic hardening as a function of plastic volumetric strains. A  
373 second contribution is then added, inspired by [Li and Dafalias \(2000\)](#), which takes into  
374 account  $\eta$ ,  $M$  and  $\psi$ . This second term defines whether the material hardens ( $H > 0$ ) or  
375 softens ( $H < 0$ ). It is also worth mentioning that  $H$  can be nil either if (i)  $M = \eta$  and  $\psi = 0$   
376 or (ii) if  $M/\eta = \exp(h_2 \psi)$ . In the former case, the material is at critical state, whereas in  
377 the second one the material is at failure.

### 378 *Parameter calibration*

379 To calibrate the CBC model, the values of eight constitutive parameters, as well as  $e_0$   
380 and  $p'_{s0}$ , have to be defined. Since the CBC model is intended to be an extension of the  
381 MMC model, the values of  $e_0$ ,  $\nu$ ,  $\kappa$ ,  $\lambda$ ,  $M$  and  $p'_{s0}$  were kept the same as before. For the sake  
382 of simplicity, it was assumed that  $g_1$ ,  $h_1$  and  $h_2$  do not depend on the C/B ratio value.

383 The parameter  $h_1$  may be calibrated independently from the other parameters on oedome-  
384 ter test results, relying on the fact that under oedometer compression neither the obliquity  
385 of the stress path nor the state parameter  $\psi$  change. For the sake of clarity, the influence  
386 of  $h_1$  on the CBC model predictions is illustrated in Figure 12a. In the same figure the  
387 experimental results (corresponding to the CB5 specimen) are also reported. A satisfactory



388 agreement with experimental data was obtained using  $h_1=0.75$ .

389 The non-dimensional parameters  $g_1$  and  $h_2$  are related to the peak value in the  $q - \varepsilon_a$   
390 plane and to the slope of the post peak branch of the curve in the  $q - \varepsilon_a$  plane, respectively.  
391 The influence of  $g_1$  and  $h_2$  on the CBC model predictions (where  $h_1=0.75$  and  $\Gamma=11.5$ ) is  
392 illustrated in Figures 12b and 12c, respectively. In the same figures, the experimental results  
393 (corresponding to the CB5 mixture) are also reported. The agreement between experimental  
394 data and model predictions is satisfactory for  $g_1=0.05$  and for  $h_2=0.1$ .

395 The  $\Gamma$  values were calibrated on the experimental results, to correctly reproduce dila-  
396 tion and compaction obtained when the confining pressure was lower or larger than the  
397 preconsolidation stress, respectively.

398 The comparison between experimental triaxial test results (points) and model predictions  
399 (dashed lines) after parameter calibration (their values are reported in Table 4) is provided  
400 in Figures 8-11. In particular, the results corresponding to the mixtures CB4, CB5 and CB6  
401 are reported in Figures 8, 9 and 10, respectively, whereas in Figure 11 the model predictions  
402 are compared with the experimental results of [Carreto et al. \(2016\)](#). **As it is evident,**  
403 **in all the cases considered the proposed constitutive relationship is capable of**  
404 **reproducing both the initial and the post-peak response: the maximum error in**  
405 **case mixture CB4, CB5 and CB6 are considered is smaller than 10%, whereas for**  
406 **mixture A of Carreto et al., 2016 is approximately 15% (for a confining pressure**  
407 **equal to 400kPa).** By summarizing, Figures 8-11 put in evidence that, with respect to  
408 MMC model, for the CBC model only one parameter more ( $\Gamma$ ) has to be calibrated. The  
409 parameter values reported in Table 4 put in evidence that the  $\Gamma$  value is decreasing with  
410 C/B and it is not significantly affected by the W/B ratio value.

## 411 **CONCLUDING REMARKS**

412 In this paper, the results of experimental tests to investigate the mechanical behavior of  
413 cement-bentonite mixtures were discussed. Even though these mixtures are realized start-  
414 ing from bentonite slurries, the microstructure of these materials is dominated by silt-sized

415 elements composed of clay aggregates and cement, partially connected one to the other by  
416 means of cementation bonds. **The link between the peculiar microstructure of the**  
417 **cement-bentonite mixture and its mechanical responses here highlighted, with**  
418 **particular attention to the presence of clusters of particles and the bonding be-**  
419 **tween them. Bonding mainly acts causing an increase in the yield stress that**  
420 **is not linked with previous stress history. The presence of clusters implies a**  
421 **response upon shearing that enhances dilation at low confining stresses and con-**  
422 **traction at larger confining stresses, as generally obtained for cement-stabilized**  
423 **clays (Miura et al. 2001).** In fact, as suggested by the undrained triaxial test experi-  
424 mental results, at high confining stresses, the undrained response is characterized by a peak  
425 in the deviatoric stress, followed by a strength loss, in analogy with the behavior of loose  
426 granular materials. Moreover, from the experimental test results it can be concluded: (i)  
427 by increasing the water/bentonite mass ratio the initial void ratio and the compliance of  
428 the material increase, while the preconsolidation pressure decreases, (ii) by increasing the  
429 cement/bentonite mass ratio the initial void ratio decreases, the preconsolidation pressure  
430 increases, while the friction angle at critical state and the logarithmic compliance slightly  
431 decrease.

432 To reproduce the mechanical response of the mixtures, two different constitutive rela-  
433 tionships were proposed: the Modified Cam Clay Model, and an original enhancement of  
434 the same model. Both the constitutive models can capture the previously cited dependence  
435 of the material properties on the mixture composition. The Modified Cam Clay model is  
436 suitable for reproducing the response up to the failure, but it cannot capture the post peak  
437 behavior. Therefore, this model may fruitfully be adopted in preliminary assessments, e.g.  
438 to verify whether, under in situ stress conditions, cracks may develop in cement bentonite  
439 cutoff walls. On the contrary, for more advanced analyses, e.g. in case the designers are  
440 interested to assess the crack size and geometrical distributions, the employment of the  
441 new constitutive relationship CBC is suggested. **The novel model was developed by**

442 joining the information at both the microstructural and laboratory scale in a  
443 unique framework, using conceptual tools widely accepted by the geotechnical  
444 community.

#### 445 **Data availability**

446 Some or all data, models, or code that support the findings of this study are available  
447 from the corresponding author upon reasonable request. These include:

- 448 • numerical results of the simulations plotted in the manuscript;
- 449 • experimental data plotted in the manuscript;
- 450 • numerical code for the integration of the constitutive law.

#### 451 **Acknowledgments**

452 The activity of the first author was financed in the context of the public administration  
453 agreement between Politecnico di Milano - Department of Civil and Environmental Engineer-  
454 ing and the Italian Ministry of Economic Development, Direzione Generale per la Sicurezza  
455 anche Ambientale delle Attività Minerarie ed Energetiche – Ufficio Nazionale Minerario per  
456 gli Idrocarburi e le Georisorse – Programme Clypea, which is here gratefully acknowledged.

## APPENDIX I. NOTATION

*The following symbols are used in this paper:*

$B$  = Bentonite mass;

$C$  = Cement mass;

$c'_p$  = cohesion intercept;

$d$  = Dilatancy;

$C_c, C_s$  = Compression index and swelling index;

$e, e_0$  = Void ratio, initial void ratio;

$f$  = Yield function;

$G_s$  = Specific gravity;

$g$  = Plastic potential function;

$g_1$  = Model parameter;

$H$  = Hardening modulus;

$h_1, h_2$  = Model parameters;

$I$  = Peak failure envelope intercept in the  $q-p'$  plane;

$K$  = Elastic bulk modulus;

$M$  = Slope of the critical state line in the  $q - p'$  plane;

$p'$  = Effective mean stress;

$p_c$  = Confining pressure;

$p_{ref}$  = Reference pressure (1 kPa);

$p'_s, p'_{s0}$  = Hardening variable and initial value of  $p'_s$ ;

$q$  = Deviator stress;

$W$  = Water mass;

$w$  = Water content;

$\Gamma$  = Critical void ratio for  $p' = p_{ref}$ ;

$\Delta u$  = Pore water pressure accumulated during triaxial test;

$\varepsilon_a, \varepsilon_{vol}^{pl}$  = Axial strain, volumetric plastic strain;

- 484  $\eta_{max}$  = obliquity of the peak failure envelope in the  $q-p'$  plane;  
485  $\kappa$  = Unloading-reloading line inclination;  
486  $\lambda$  = Normal compression line and critical state line inclination;  
487  $\nu$  = Poisson ratio;  
488  $\sigma'_h, \sigma'_v$  = Horizontal and vertical effective stress;  
489  $\phi'_{cv}, \phi'_p$  = Constant volume and peak friction angle  $\psi$  = State parameter

## REFERENCES

- Atkinson, J. H. and Bransby, P. L. (1978). *The mechanics of soils: an introduction to critical state soil mechanics*. McGraw-Hill Book Co.
- Azizi, A., Musso, G., and Jommi, C. (2020). “Effects of repeated hydraulic loads on microstructure and hydraulic behaviour of a compacted clayey silt.” *Canadian Geotechnical Journal*, 57(1), 100–114.
- Been, K. and Jefferies, M. G. (1985). “A state parameter for sands.” *Géotechnique*, 35(2), 99–112.
- Carreto, J. M. R., Caldeira, L. M. M. S., and Neves, E. J. L. M. D. (2016). “Hydromechanical characterization of cement-bentonite slurries in the context of cutoff wall applications.” *Journal of Materials in Civil Engineering*, 28(2), 04015093.
- Dafalias, Y. F. and Manzari, M. T. (2004). “Simple plasticity sand model accounting for fabric change effects.” *Journal of Engineering mechanics*, 130(6), 622–634.
- Delage, P. and Pellerin, F. (1984). “Influence de la lyophilisation sur la structure d’une argile sensible du québec.” *Clay minerals*, 19(2), 151–160.
- Jefferis, S. (2012). “Cement-bentonite slurry systems.” *Grouting and Deep Mixing 2012*, 1–24.
- Jefferis, S. A. (1981). “Bentonite-cement slurries for hydraulic cut-offs.” *Proceedings, Tenth International Conference on Soil Mechanics and Foundation Engineering, Stockholm, Sweden*, Vol. 1, 435–440.
- Joshi, K., Kechavarzi, C., Sutherland, K., Ng, M. Y. A., Soga, K., and Tedd, P. (2010). “Laboratory and in situ tests for long-term hydraulic conductivity of a cement-bentonite cutoff wall.” *Journal of geotechnical and geoenvironmental engineering*, 136(4), 562–572.
- Kang, X., Kang, G. C., Chang, K. T., and Ge, L. (2015). “Chemically stabilized soft clays for road-base construction.” *Journal of Materials in Civil Engineering*, 27(7), 04014199.
- Li, X. S. and Dafalias, Y. F. (2000). “Dilatancy for cohesionless soils.” *Geotechnique*, 50(4), 449–460.
- Manzari, M. T. and Dafalias, Y. F. (1997). “A critical state two-surface plasticity model for

sands.” *Geotechnique*, 47(2), 255–272.

Miura, N., Horpibulsuk, S., and Nagarj, T. (2001). “Engineering behavior of cement stabilized clay at high water content.” *Soils and Foundations*, 41(5), 33–45.

Musso, G., Azizi, A., and Jommi, C. (2020a). “A microstructure-based elastoplastic model to describe the behaviour of a compacted clayey silt in isotropic and triaxial compression.” *Canadian Geotechnical Journal*, 57, 1025–1043.

Musso, G., Zibisco, A., Cosentini, R. M., Trischitta, P., and Della Vecchia, G. (2020b). “Monitoring drying and wetting of a cement bentonite mixture with electrical resistivity tomography.” *Proceedings of the 4th European Conference on Unsaturated Soil Mechanics, Lisbon, October 2020*.

Opdyke, S. M. and Evans, J. C. (2005). “Slag-cement-bentonite slurry walls.” *Journal of geotechnical and geoenvironmental Engineering*, 131(6), 673–681.

Plee, D., Lebedenko, F., Obrecht, F., Letellier, M., and Van Damme, H. (1990). “Microstructure, permeability and rheology of bentonite - cement slurries.” *Cement and Concrete Research*, 20(1), 45–61.

Roscoe, K. and Burland, J. B. (1968). “On the generalized stress-strain behaviour of wet clay.” *In Engineering plasticity, Cambridge, UK: Cambridge University Press*, 535–609.

Royal, A., Makhover, Y., Moshirian, S., and Hesami, D. (2013). “Investigation of cement–bentonite slurry samples containing pfa in the ucs and triaxial apparatus.” *Geotechnical and Geological Engineering*, 31(2), 767–781.

Royal, A., Opukumo, A., Qadr, C., Perkins, L., and Walenna, M. (2018). “Deformation and compression behaviour of a cement–bentonite slurry for groundwater control applications.” *Geotechnical and Geological Engineering*, 36(2), 835–853.

Soga, K., Joshi, K., and Evans, J. (2013). “Cement bentonite cutoff walls for polluted sites.” *Proceedings of the 1st international symposium on Coupled Phenomena in Geotechnical Engineering, Manassero et al. (Eds), Taylor Francis Group, London*, 149–165.

Tarzia, S. (2018). *Hydraulic behaviour of cement bentonite mixtures*. MSc thesis, Politecnico

544 di Torino (in Italian).

545 Trischitta, P., Cosentini, R. M., Della Vecchia, G., Sanetti, G., and Musso, G. (2020). “Pre-

546 liminary investigation on the water retention behaviour of cement bentonite mixtures.”

547 *Proceedings of the 4th European Conference on Unsaturated Soil Mechanics, Lisbon, Oc-*

548 *tober 2020.*

549 van Olphen, H. (1977). *An introduction to clay colloid chemistry, for clay technologists,*

550 *geologists, and soil scientists.* 2nd edition John Wiley & Sons, p. 318.



551

**List of Tables**

552        1    Cement-bentonite mixture composition . . . . . 25

553        2    Ultimate and peak envelope parameters . . . . . 26

554        3    Modified Cam Clay parameters . . . . . 27

555        4    Constitutive model parameters . . . . . 28

**TABLE 1.** Cement-bentonite mixture composition

Mixture	Mass ratio at preparation		Properties after 28 days of curing		
	Water/bentonite [-]	Cement/bentonite [-]	Water content $w$ [%]	Specific gravity $G_s$ [-]	Initial void ratio $e_0$ [-]
CB 4	18/1	4/1	306	2.88	8.8
CB 5	18/1	5/1	264	2.76	7.29
CB 6	18/1	6/1	230	2.72	6.25

**TABLE 2.** Ultimate and peak envelope parameters

Mixture	Critical state			Peak		
	$M[-]$	$\phi'_{cv} [^\circ]$	$\eta_{max} [-]$	$I [kPa]$	$\phi'_p [^\circ]$	$c'_p [kPa]$
CB 4	2.00	49.00	-	-	-	-
CB 5	1.96	47.75	2.03	15	49.30	7
CB 6	1.84	44.87	1.82	17	44.36	9

**TABLE 3.** Modified Cam Clay parameters

	$e_0$ [-]	$\nu$ [-]	$\kappa$ [-]	$\lambda$ [-]	$M$ [-]	$p'_{s0}$ [kPa]
CB4	8.8	0.25	0.06	1.5	2	30
CB5	7.29	0.25	0.06	1.35	1.96	65
CB6	6.25	0.25	0.06	1.2	1.84	110
mixture A <a href="#">Carreto et al. (2016)</a>	8.58	0.25	0.09	1.45	2	25

**TABLE 4.** Constitutive model parameters

	$e_0$ [-]	$\nu$ [-]	$\kappa$ [-]	$\lambda$ [-]	$M$ [-]	$p'_{s0}$ [kPa]	$g_1$ [-]	$h_1$ [-]	$h_2$ [-]	$\Gamma$ [-]
CB4	8.8	0.25	0.06	1.5	2	30	0.05	0.75	0.1	12.8
CB5	7.29	0.25	0.06	1.35	1.96	65	0.05	0.75	0.1	11.5
CB6	6.25	0.25	0.06	1.2	1.84	110	0.05	0.75	0.1	10.2
A of <a href="#">Carreto et al. (2016)</a>	8.58	0.25	0.09	1.45	2	25	0.05	0.75	0.1	11

556

## List of Figures

557	1	Molds for the preparation of specimens for oedometer testing (left, internal	
558		diameter 50.5 mm and height 20 mm) and for triaxial tests (right, internal	
559		diameter 38.1 mm and height 76.2 mm ) . . . . .	30
560	2	SEM images at different magnifications of a CB5 specimen after 28 days of	
561		curing . . . . .	31
562	3	Atomic composition detected during SEM testing through Energy Dispersive	
563		X-ray microanalysis. Numbers above each spectrum refer to the position in	
564		the bottom left image of Figure 2 . . . . .	32
565	4	Experimental compression curves in oedometer for the three cement-bentonite	
566		mixtures . . . . .	33
567	5	TXCU test results for confining pressure equal to a) 20kPa, b) 100kPa and	
568		300kPa . . . . .	34
569	6	Experimental determination of peak and ultimate envelope: a) CB4, b) CB5	
570		and c) CB6 . . . . .	35
571	7	Calibration of the MMC model parameters in the $e - \sigma'_v$ plane: a) mixture	
572		CB4, b) mixture CB5 and c) mixture CB6 . . . . .	36
573	8	Comparison between experimental results and constitutive model prediction	
574		(mixture CB4) . . . . .	37
575	9	Comparison between experimental results and constitutive model prediction	
576		(mixture CB5) . . . . .	38
577	10	Comparison between experimental results and constitutive model prediction	
578		(mixture CB6) . . . . .	39
579	11	Comparison between experimental results and constitutive models prediction	
580		(mixture A in Carreto et al. (2016)) . . . . .	40
581	12	Calibration of the parameters of the CBC model: a) $h_1$ , b) $g_1$ and c) $h_2$ . . .	41

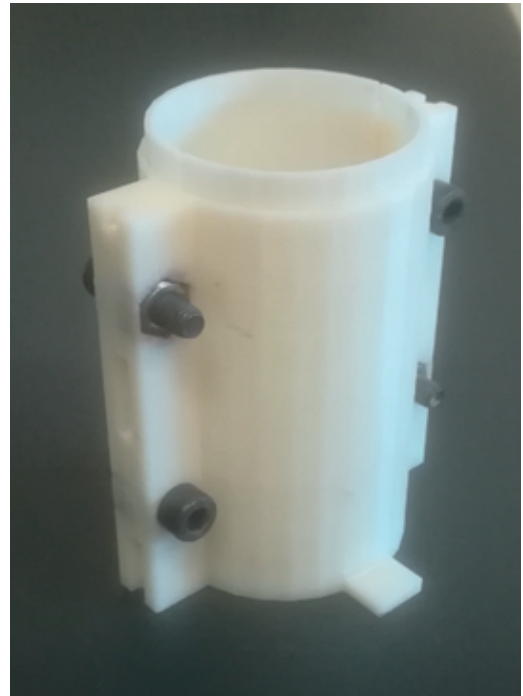


**Fig. 1.** Molds for the preparation of specimens for oedometer testing (left, internal diameter 50.5 mm and height 20 mm) and for triaxial tests (right, internal diameter 38.1 mm and height 76.2 mm )

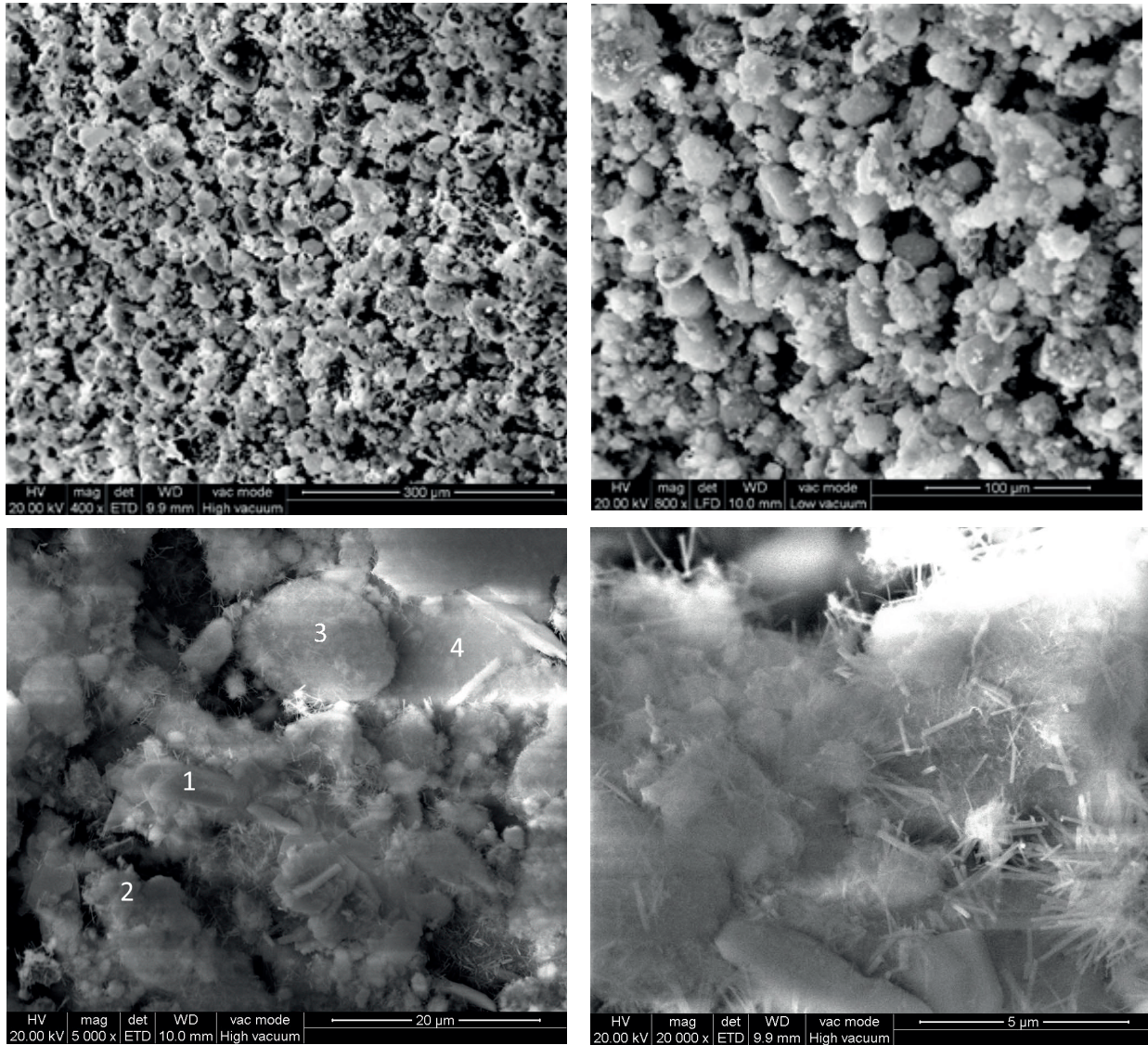


**Fig. 2.** SEM images at different magnifications of a CB5 specimen after 28 days of curing



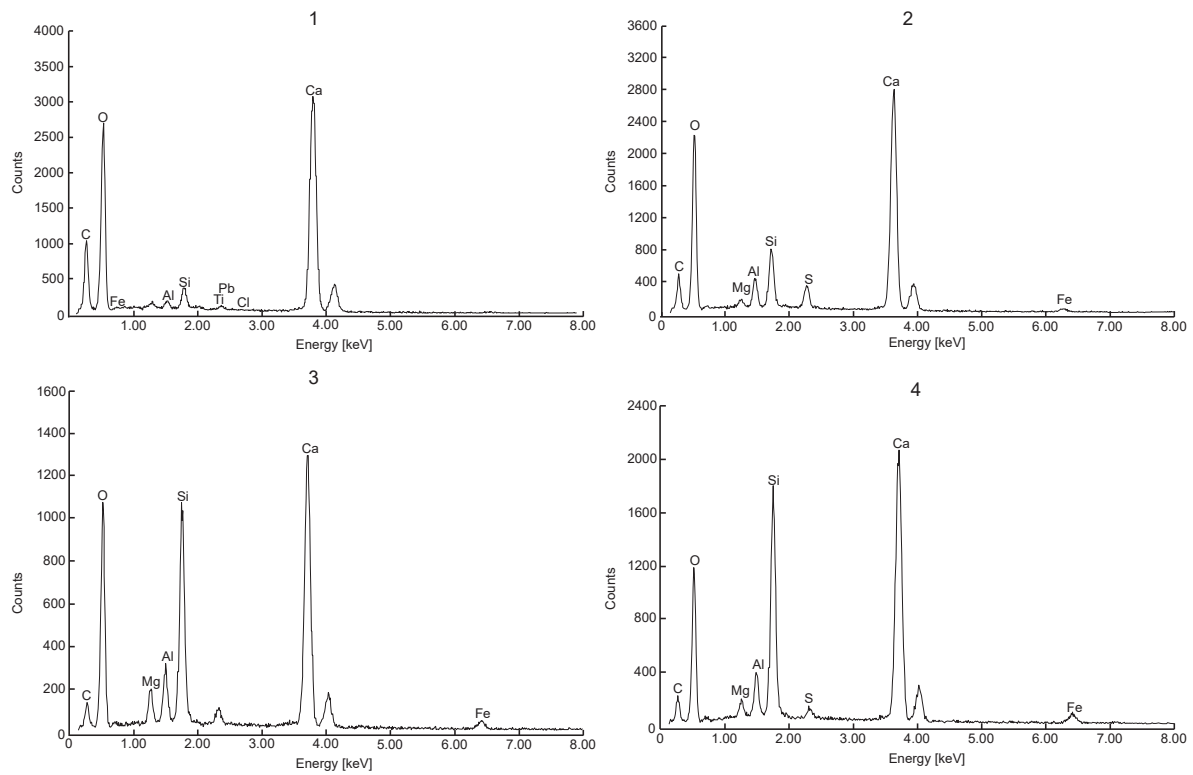


**Fig. 3.** Atomic composition detected during SEM testing through Energy Dispersive X-ray microanalysis. Numbers above each spectrum refer to the position in the bottom left image of Figure 2

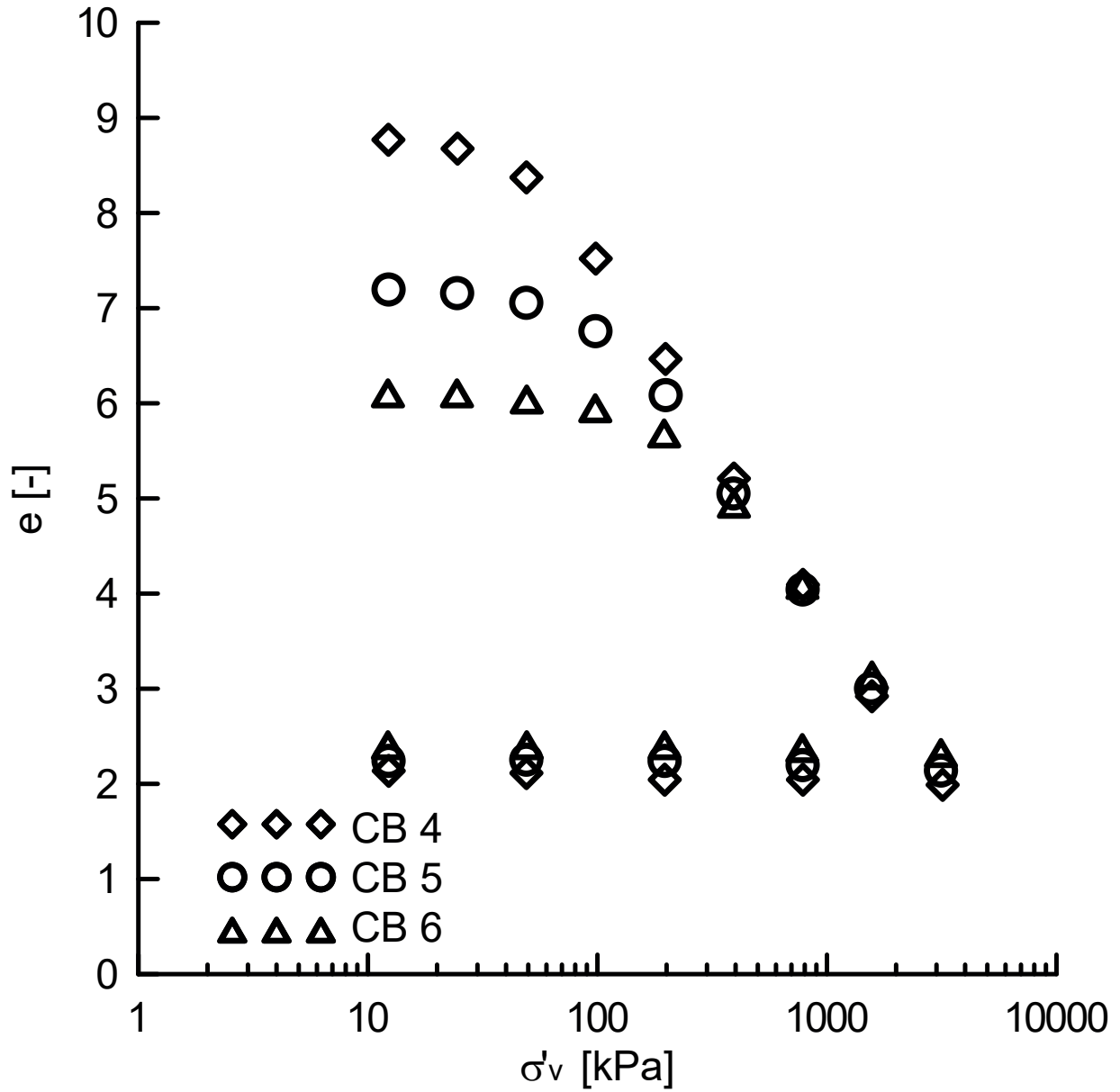


**Fig. 4.** Experimental compression curves in oedometer for the three cement-bentonite mixtures

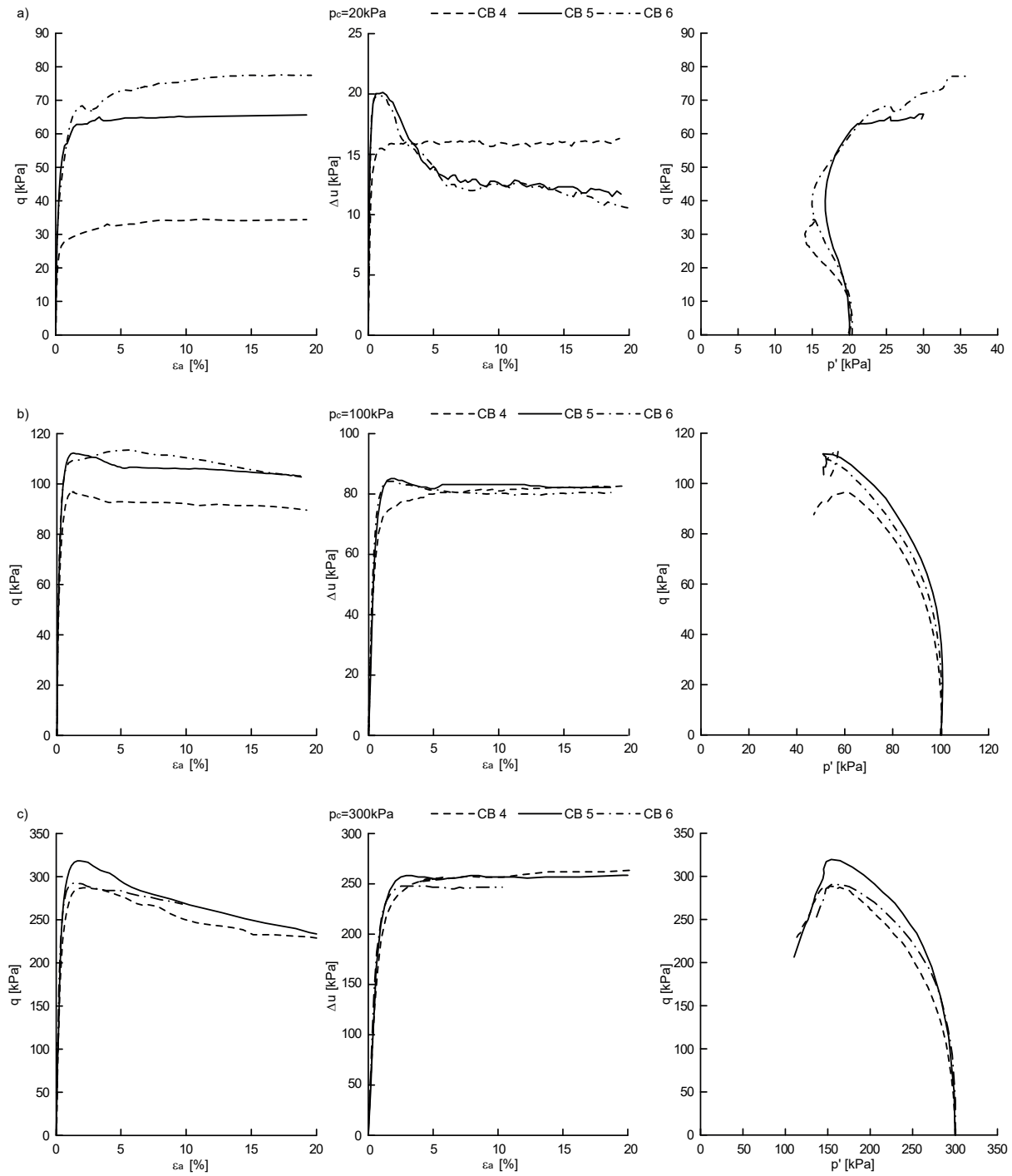


**Fig. 5.** TXCU test results for confining pressure equal to a) 20kPa, b) 100kPa and c) 300kPa

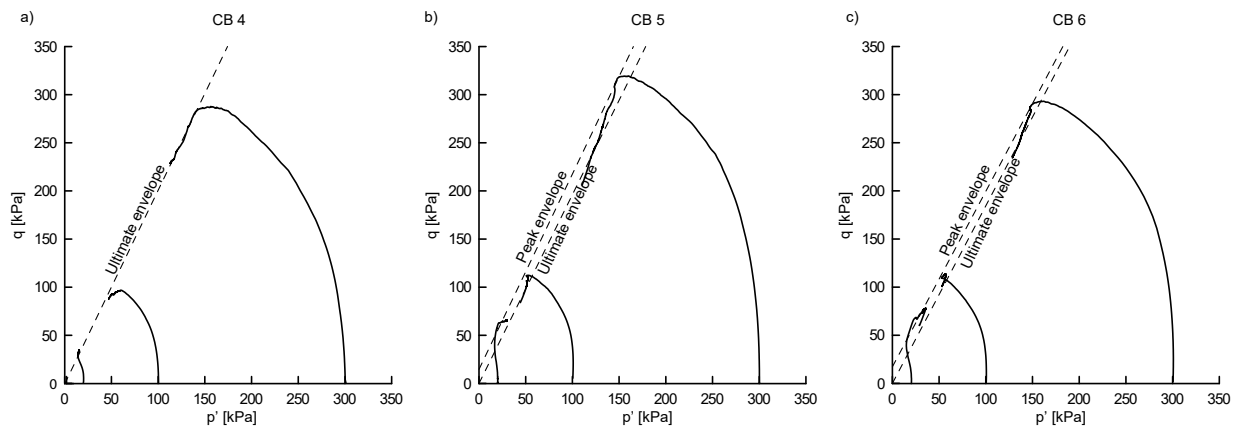


**Fig. 6.** Experimental determination of peak and ultimate envelope: a) CB4, b) CB5 and c) CB6

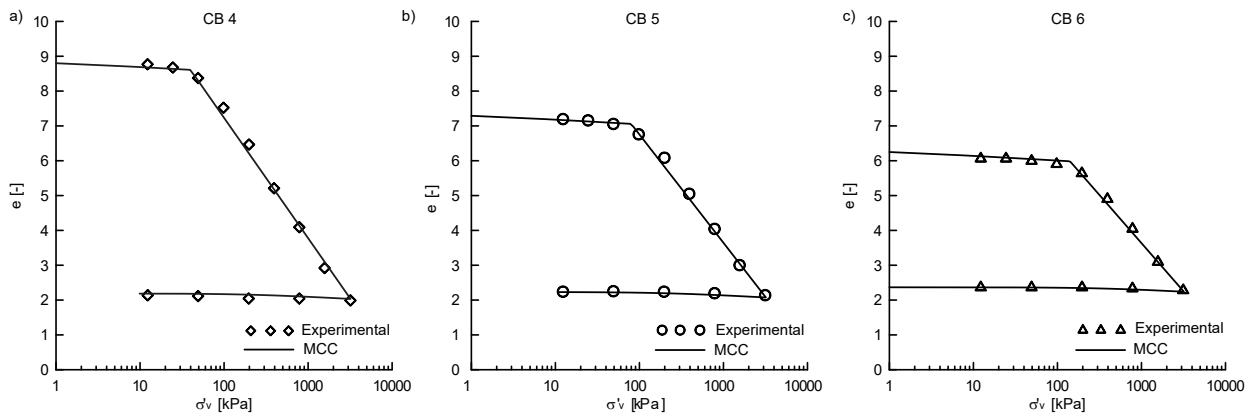


**Fig. 7.** Calibration of the MMC model parameters in the  $e - \sigma'_v$  plane: a) mixture CB4, b) mixture CB5 and c) mixture CB6

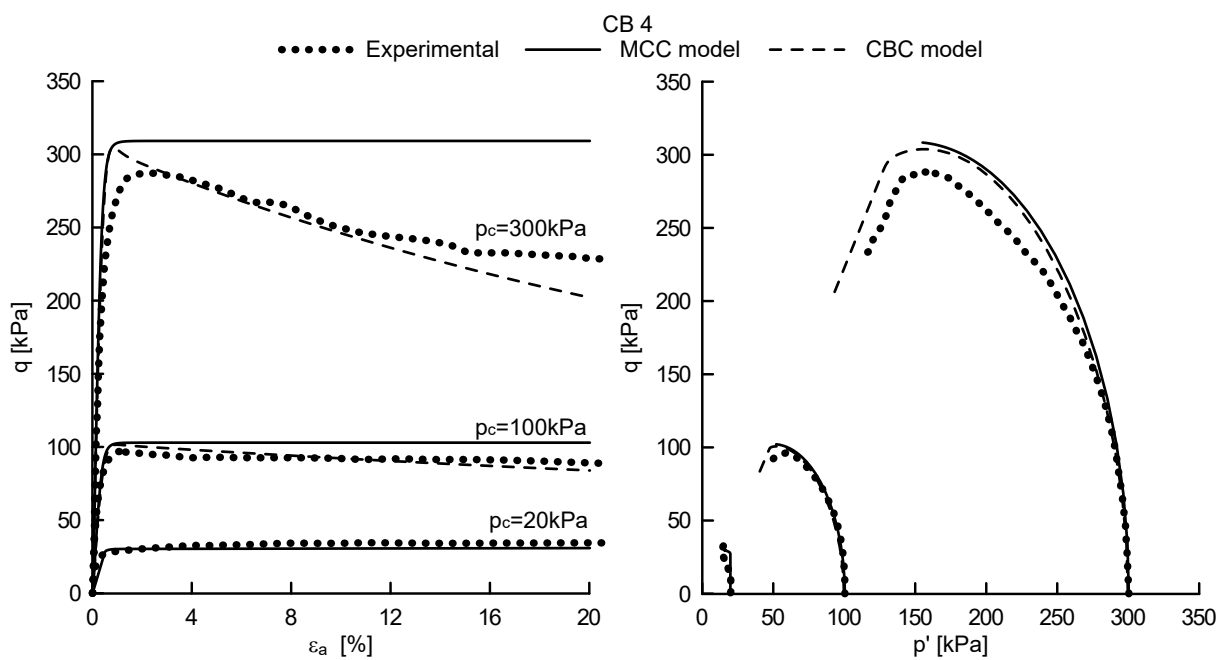


**Fig. 8.** Comparison between experimental results and constitutive model prediction (mixture CB4)

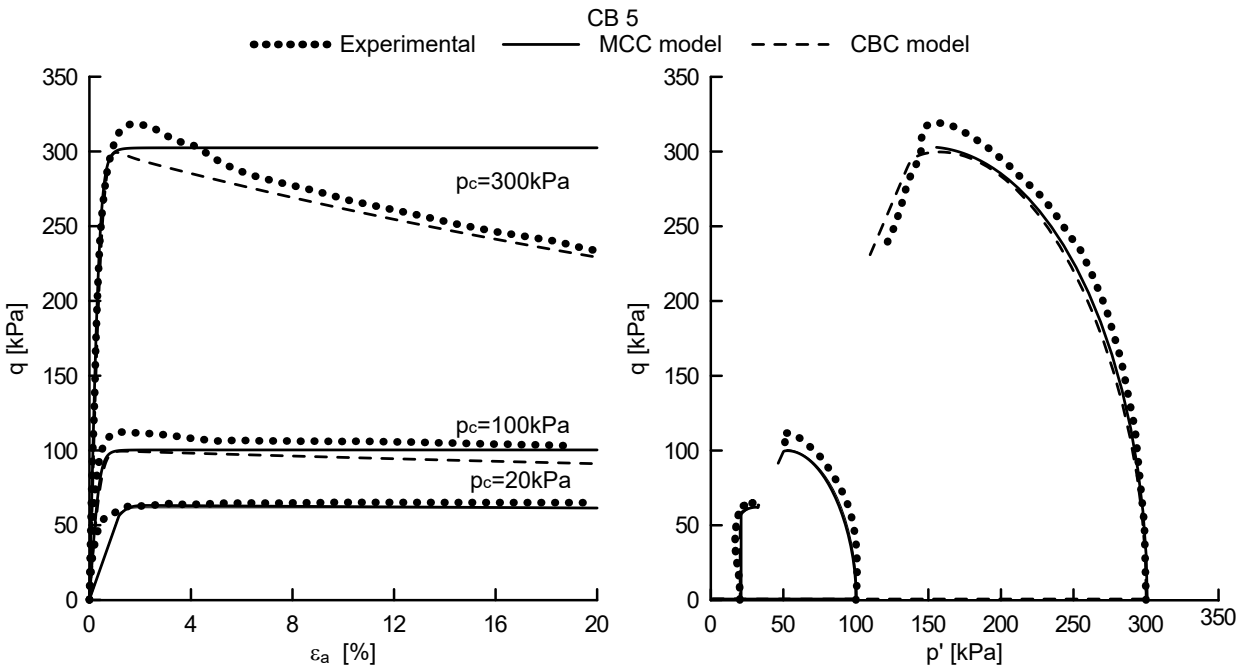


**Fig. 9.** Comparison between experimental results and constitutive model prediction (mixture CB5)

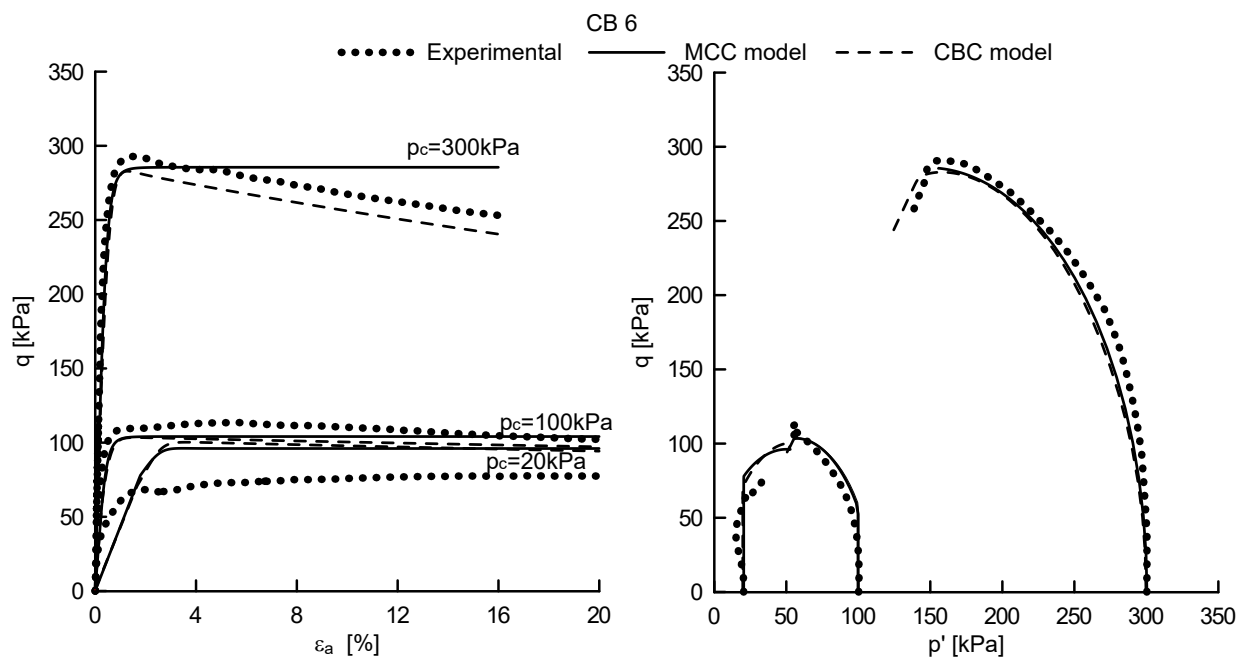


**Fig. 10.** Comparison between experimental results and constitutive model prediction (mixture CB6)



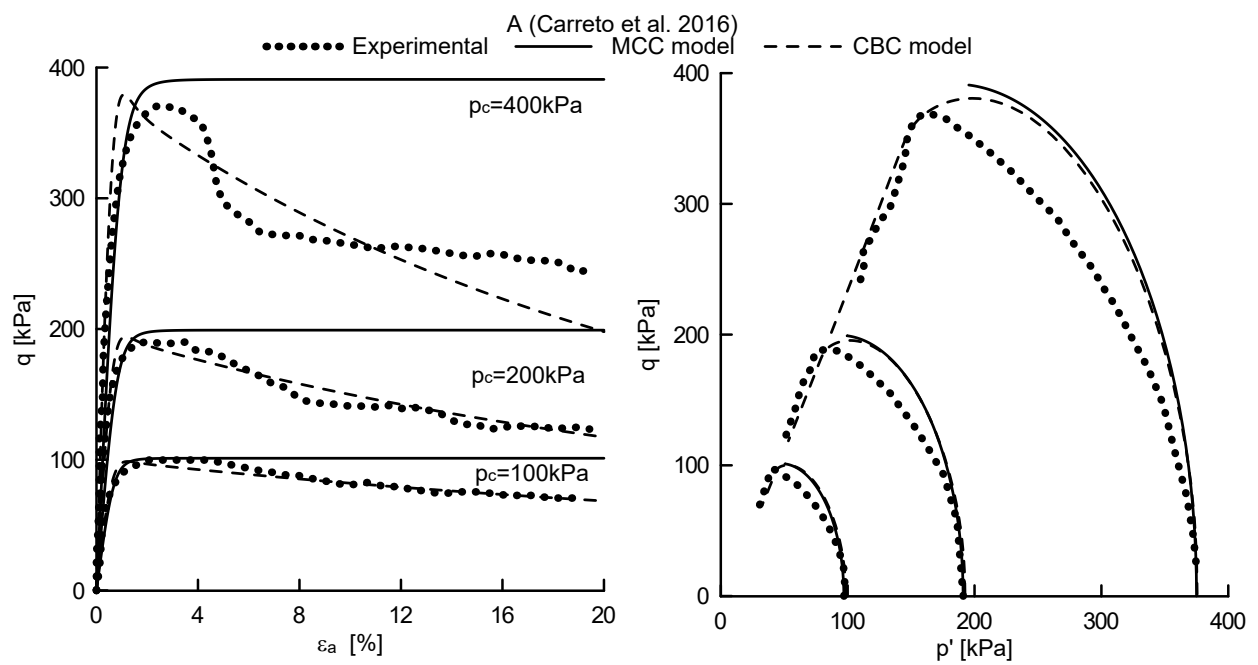


**Fig. 11.** Comparison between experimental results and constitutive models prediction (mixture A in Carreto et al. (2016))

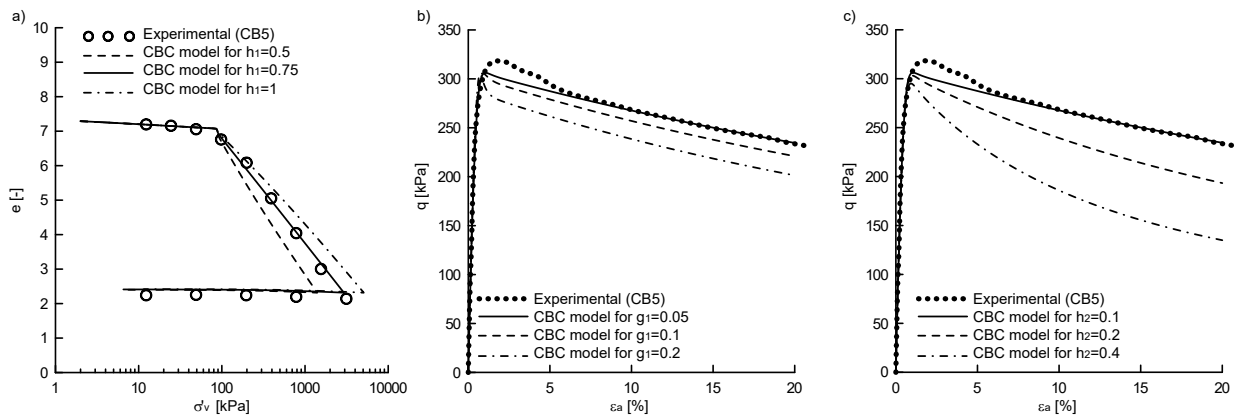


**Fig. 12.** Calibration of the parameters of the CBC model: a)  $h_1$ , b)  $g_1$  and c)  $h_2$